Materials Research Express

PAPER • OPEN ACCESS

Enhanced dielectric properties of green synthesized Nickel Sulphide (NiS) nanoparticles integrated polyvinylalcohol nanocomposites*

To cite this article: P Lokanatha Reddy *et al* 2020 *Mater. Res. Express* **7** 064007

Materials Research Express

OPEN ACCESS

RECEIVED
9 March 2020

REVISED
15 May 2020

ACCEPTED FOR PUBLICATION
21 May 2020

PUBLISHED
10 June 2020

PAPER

Enhanced dielectric properties of green synthesized Nickel Sulphide (NiS) nanoparticles integrated polyvinylalcohol nanocomposites*

P Lokanatha Reddy[1], Kalim Deshmukh[2], Tomáš Kovářík[2], David Reiger[2], N Arunai Nambiraj[3], Lakshmipathy R[4] and Khadheer Pasha S K[5]

[1] Department of Physics, School of Advanced Sciences, VIT University, Vellore-632014, Tamil Nadu, India
[2] New Technologies-Research Center, University of West Bohemia, Pilsen-30100, Czech Republic
[3] Centre for Biomaterials, Cellular and Molecular Theranostics (CBCMT), VIT University, Vellore-632014, Tamil Nadu, India
[4] Department of Chemistry, KCG College of Technology, Karapakkam, Chennai-60009, Tamil Nadu, India
[5] Department of Physics, VIT-AP University, Amaravati, Guntur -522501, Andhra Pradesh, India

E-mail: khadheerbasha@gmail.com

Keywords: NiS NPs, green synthesis, PVA composites, thermal behaviour, morphology, dielectric properties

Abstract

A green synthesis approach has been adopted to prepare nickel sulphide nanoparticles (NiS NPs) using banana peel extract (BPE) as a reducing and capping agent. Polyvinyl alcohol (PVA)/NiS nanocomposite films were fabricated using a cost-effective solution casting technique by dispersing different contents of NiS NPs (0–3 wt%) in the PVA matrix. Various characterization techniques were employed to analyze the structural, thermal and morphological properties of the PVA/NiS nanocomposite films. Further, the dielectric behaviour of these nanocomposite films was investigated at frequency range 50 Hz–20 MHz and in the temperature range 40 °C–140 °C. Also, there exists a significant interaction between the polymer matrix and the nanofiller as evident from the notable improvement in the dielectric properties of the nanocomposites. The dielectric constant (ε) value of PVA/NiS nanocomposite film with 3 wt % NiS NPs loading was found to be 154.55 at 50 Hz and at 140 °C which is 22 times greater than the dielectric constant value of neat PVA (6.90). These results suggest that NiS NPs were dispersed homogeneously in the PVA matrix.

1. Introduction

In recent times, tremendous research interest has been devoted to the development of novel polymer nanocomposites (PNCs) because of their enhanced properties [1–3]. The PNCs reinforced with inorganic nanoparticles (NPs) have potential applications such as optical power limiters, membranes for gas separation, flexible light emitters etc [4, 5]. Polymer/filler interface, the geometry of the dispersed phase (orientation, size, shape etc), their relative contents, and also volume fraction can alter or modify the final properties of PNCs [6]. The unavailability of low-cost techniques to control the distribution of NPs into the host polymer matrix is the main obstruction to the large-scale fabrication of PNCs [7]. For the PNCs, the major limitation in the application side is that the aggregation of NPs or their distribution in the polymer matrix. So, there is a necessity that the NPs have to be dispersed homogeneously within the polymer matrix because it causes an improvement in the chemical and physical properties of the PNCs [8, 9]. Therefore, to control the functioning of PNCs, two important parameters are required i.e., the spatial distribution of NPs and their interactions with the host polymer matrix [10–12]. For the past few years, it has been considered that the improved dielectric properties of the PNCs loaded with inorganic NPs is believed to be a strong candidate for energy storage applications [13, 14]. Some of the reports revealed that the dielectric properties of PNCs filled with the semiconductor NPs were enhanced when compared with pure polymers [15, 16].

* This work was presented at the 2nd International Conference on Nanoscience and Nanotechnology (ICNAN'19)' at VIT University, Vellore (India) from 29th Nov–1st Dec. 2019. Chairman: Prof. A. Nirmala Grace.

Among various polymers used for the fabrication of PNCs, polyvinyl alcohol (PVA) is most often preferred as a host matrix owing to its excellent film-forming ability, higher dielectric strength, the capability to form strong hydrogen bonding, easy processability, excellent chemical stability, and highly durable nature [17]. PVA has been employed for various applications such as in battery components, packaging, textile applications in the microelectronic industry, electromagnetic interference applications and so on [17, 18]. Several research groups reported the dielectric properties of the PVA based nanocomposites [19–21]. With this inspiration, in the present study PVA has been chosen as a host polymer to synthesize PVA based nanocomposites. Now a day, more attention has been focussed on metal sulphide nanostructures because of their unique properties and applications [22]. Among these, nickel sulphide (NiS) has been mostly investigated because of its simple production, affordable price and high electronic conductivity [23, 24]. It exhibits complicated electrical, optical, structural, compositional and magnetic phase behaviour [25]. Also due to the possession of multi-phases, binary Ni–S systems such as NiS_2, Ni_3S_4, Ni_9S_8, Ni_7S_6, Ni_6S_5, Ni_4S_{3+x}, Ni_3S_2, and $Ni_{3+x}S_2$ have become fascinated materials [26]. NiS NPs exhibit different shapes such as layer-rolled structures, urchin-like nanocrystallites, flower-like architectures, hollow spheres, nanoframes, nanorods, and nanospheres etc [27, 28].

Recently, increased attention has been given to the green approach for the synthesis of NPs because of its several advantages [29–32]. For the synthesis of NPs, the plant extracts which serve as reducing/capping agents are considered to be more beneficial than remaining techniques [33]. Several researchers reported the synthesis of metal sulphide NPs through a green synthesis approach using extracts of different parts of plants as reducing/capping agents [34, 35]. Bananas are cultivated almost all over the world. Banana peels are potentially used in environmental cleaning, organic fertilizer, energy-related activities, cosmetics, pulp and paper making, bio-sorbents, bio-fuel manufacturing etc [36]. Banana peels are intrinsically affluent in polymers like pectin, carbohydrates, hemicelluloses, cellulose, and lignin which have been utilized as reducing/capping materials for the synthesis of NPs [37, 38]. Some reports revealed the usage of various green synthesized materials for a wide range of applications [39]. With this interest, here banana peel extract (BPE) has been selected as a reducing/capping agent to prepare the NiS NPs. Subsequently, the NiS NPs were used as nanofiller to prepare PVA/NiS nanocomposites.

The main aim of the present study to synthesize the NiS NPs using a green synthesis approach followed by their incorporation into the PVA matrix for the preparation of PVA/NiS nanocomposite films via the solution casting method. Besides, the structural, thermal, morphological and dielectric properties of the prepared nanocomposites were investigated using various characterization techniques.

2. Experimental

2.1. Materials

Fresh banana peels were obtained from banana agricultural fields. Sodium sulphide (Na_2S), nickel nitrate hexahydrate ($Ni(NO_3)_2{\cdot}6H_2O$), PVA powder (MW = 85,000–1,24,000 g $mole^{-1}$ with 87%–89% degree of hydrolysis) and N, N-Dimethylformamide (DMF) were received from Sigma-Aldrich, India.

2.2. Preparation of BPE

First, banana peels were cleaned using deionized (DI) water to take away unwanted organic impurities and dust present in it. Subsequently, these peels were dried on paper towel. Then, appropriate quantity of peel was heated at 90 °C in a beaker containing DI water and subsequently filtered. This obtained filtrate was utilized as reducing or capping agent to synthesize NiS NPs.

2.3. Synthesis of NiS NPs

Green synthesis approach was employed to prepare the NiS NPs. $Ni(NO_3)_2{\cdot}\,6H_2O$ was used as nickel ions source and Na_2S was used for obtaining the sulphide ions. 1M $Ni(NO_3)_2{\cdot}\,6H_2O$ and 1M Na_2S were dissolved in DI water separately and stirred using magnetic stirrer for one hour at room temperature (RT) to obtain clear solution. Subsequently, both the solutions were mixed and stirred for additional one hour to get homogeneous solution. In this solution, an appropriate quantity of BPE was added and stirred for 6 h at 70 °C. After that as obtained precipitate was washed several times using DI water and ethanol to eliminate the unwanted impurities or residues. The final material was dried in hot air oven at 95 °C for 24 h and subsequently in muffle furnace at 300 °C for 2 h [40]. Finally, the black powder was obtained which was grinded using mortar and pestle and utilised for the synthesis of PVA/NiS nanocomposites.

2.4. Preparation of PVA/NiS nanocomposite films

Figure 1 schematically represents the preparation procedure of PVA/NiS nanocomposite films using solution casting technique. The desired amount of PVA solution was obtained by dissolving PVA powder in DI water by

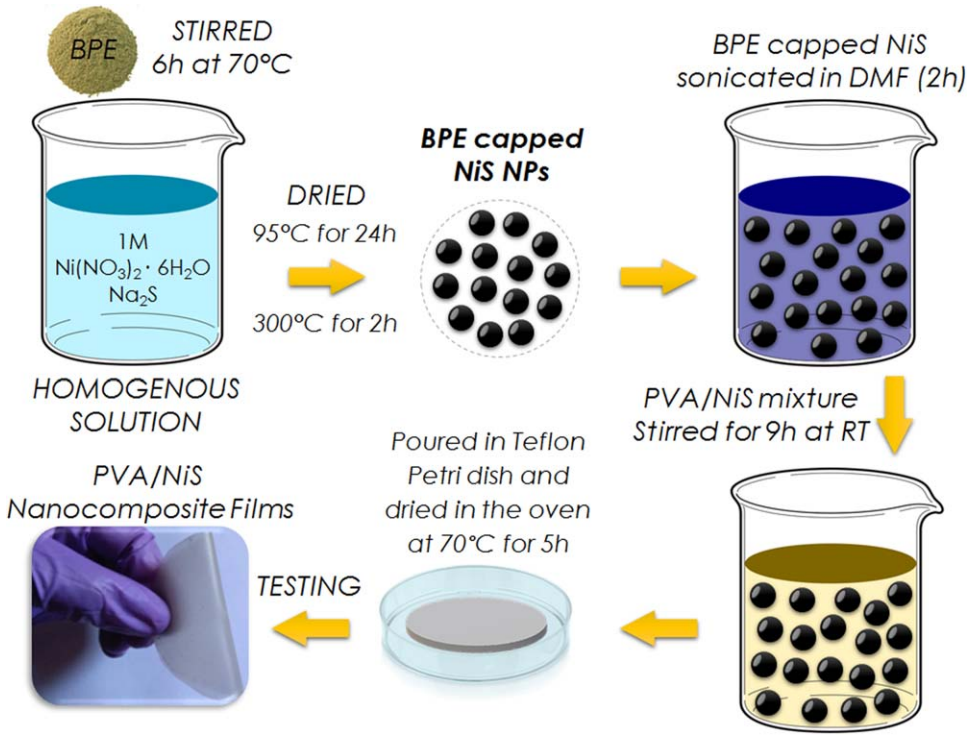

Figure 1. Representation of the synthesis protocol of PVA/NiS nanocomposite films.

heating at 65 °C in hot air oven for 3 h. The NiS NPs were dispersed in DMF, sonicated for two hours and then mixed with PVA solution. Further, PVA/NiS mixture was constantly stirred for 9 h until the uniform distribution of NiS NPs in PVA is ensured. This resultant dispersion was poured onto Petri dish, afterwards kept at 70 °C in hot air oven for 5 h to obtain nanocomposite films. These PVA/NiS nanocomposite films having 70–80 μm thickness was peeled off from Petri dish and used for further characterizations.

2.5. Characterizations

Fourier transform infrared spectroscopy (Japan, Shimadzu, IRaffinity-1) was employed to measure FTIR transmittance spectra of NiS NPs, neat PVA and PVA/NiS nanocomposites in the wavenumber range 4000–400 cm^{-1}.

X-ray diffraction experiments were performed usingan x-ray diffractometer (Germany, Bruker, Advanced D8) with a wavelength of 1.54 Å and 1° min^{-1} scanning speed using Cu Kα radiation. The recorded data was obtained in 2θ ranging from 10–90°.

Thermogravimetric analysis (TGA) of the prepared samples was performed from RT to 800 °C using TGA thermal analyzer (USA, TA Instruments, Q500 model) and differential scanning calorimeter (DSC) (TA Instruments, Q200 model) from RT to 400 °C at the heating rate of 10 °C min^{-1} in a N_2 atmosphere.

Crossed polarizing optical microscope (POM) (Singapore, BX-53, Olympus) with a magnification 10X was employed to assess the dispersion state of NiS NPs in the PVA matrix.

Scanning electron microscopy (SEM) (UK, Carl Zeiss EVO/18SH) was used to investigate the surface morphology of the samples. An accelerating voltage of 15 kV was applied for obtaining SEM images. Energy dispersive analysis of x-ray diffraction (EDAX) was coupled with the SEM to analyze the chemical compositions present in the synthesized NiS NPs.

High-resolution transmission electron microscopy (HRTEM) images of NiS NPs and PVA/NiS nanocomposite films were obtained using FEI-Tecnai G2–20 twin 200 kV spectrometer.

Precision impedance analyzer (UK, Chichester, West Sussex, Wayne Kerr 6500B) was used to test the dielectric behaviour of PVA and PVA/NiS nanocomposite films in the frequency range 50 Hz–20 MHz and the temperature range 40 °C–140 °C.

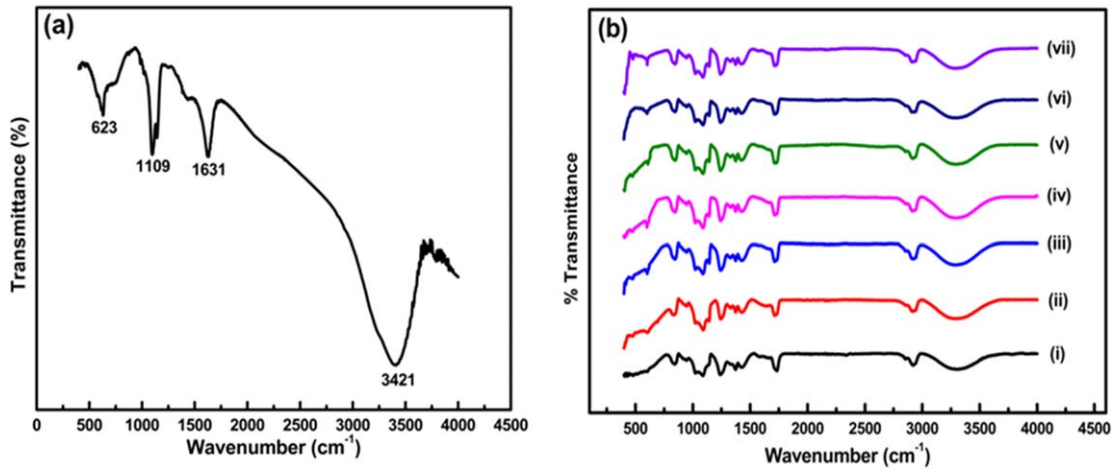

Figure 2. FTIR spectra of (a) NiS NPs and (b) (i) neat PVA, (ii) PVA/NiS nanocomposite films filled with 0.5 wt% NiS NPs, (iii) 1.0 wt% NiS NPs, (iv)1.5 wt% NiS NPs, (v) 2.0 wt% NiS NPs, (vi) 2.5 wt% NiS NPs and (vii) 3.0 wt% NiS NPs.

3. Results and discussions

3.1. FTIR study

Figure 2(a) displays the FTIR spectrum of NiS NPs. The bands appeared at 3421 and 1631 cm^{-1} are assigned to stretching and bending vibrations respectively of hydroxyl groups present on the surface of the sample [41]. The peak at 623 cm^{-1} could be assigned to bending vibration mode in Ni–S–Ni [42]. Figure 2(b) (i)–(vii) demonstrates the FTIR spectra of PVA and PVA/NiS nanocomposite films. The pure PVA (figure 2(b) (i)) depicts absorption and strong band at 3306 cm^{-1} assigned to the vibration of –OH group (stretching) [43]. The bands observed at 2916 and 1726 cm^{-1} may be attributed to C–H asymmetric stretching vibration (alkyl groups) and of C=O (vinyl acetate group) stretching vibration respectively [44]. The CH_2 bending vibration in the PVA backbone chain is represented by the band that appeared at 1431 cm^{-1} [45]. The CH_2 and C–H wagging vibrations are represented by the bands at 1363 and 1235 cm^{-1} respectively [17]. The bands at 1083 and 838 cm^{-1} are attributed to the stretching vibration of C–O in the backbone of PVA (acetyl group) and skeletal vibration in PVA respectively [46, 47]. Moreover, almost the same peaks were noticed in the FTIR spectra of PVA/NiS nanocomposites (figure 2(b) (ii)–(vii)) along with some additional peaks below 660 cm^{-1} which may be attributed to bending vibration of Ni-S-Ni [48]. However, a small shift in the peak position was noticed in the FTIR spectra of PVA/NiS nanocomposites representing good compatibility between the NiS and hydroxyl groups of PVA.

3.2. XRD analysis

Figure 3(a) depicts XRD pattern of NiS NPs indicating major diffraction peaks at $2\theta = 30.25°, 34.53°, 45.72°$ and 53.57° which corresponds to the reflections of crystal planes (100), (101), (102) and (110) match with NiS (α- phase) with space group P63/mmc (hexagonal phase, JCPDS: 075-0613) [40, 49]. Normally, peak broadening in the x-ray diffraction peaks consists of two components namely physical broadening and instrumental broadening which happens due to the effect of crystallite size and and the intrinsic strain respectively. The corrected instrumental broadening (β_{hkl}) for the peaks of NiS NPs can be written as,

$$(\beta^2_{hkl})_{\text{corrected}} = (\beta^2_{hkl})_{\text{measured}} - (\beta^2)_{\text{instrumental}} \quad (1)$$

And the crystallite size (D) can be calculated using Debye-Scherrer formula,

$$D = \frac{k\lambda}{\beta_{hkl}\ \cos\theta} \quad (2)$$

Where k is the shape factor ($k = 0.9$), λ is the wavelenth of the x-rays ($\lambda = 0.154056$ nm), β_{hkl} is the broadening of the diffraction peak measured at half of its maximum intensity and θ is the angle of diffraction [50].

From Scherrer's formula, the average crystallite size is found to be around 19 nm. But, Scherrer's formula provides only the effect of crystallite size on the peak broadening and it is just a part of the instrumental broadening function. Also, Scherrer formula doesnot give the information about the intrinsic strain which is developed in the nanocrystals because of stacking faults, triple junction, grain boundary and point defects. Here, in order to calculate two independent factors i.e. the crystallite size and intrinsic strain, uniform deformation model (UDM) in Williamson-Hall (W-H) method is used [50, 51].

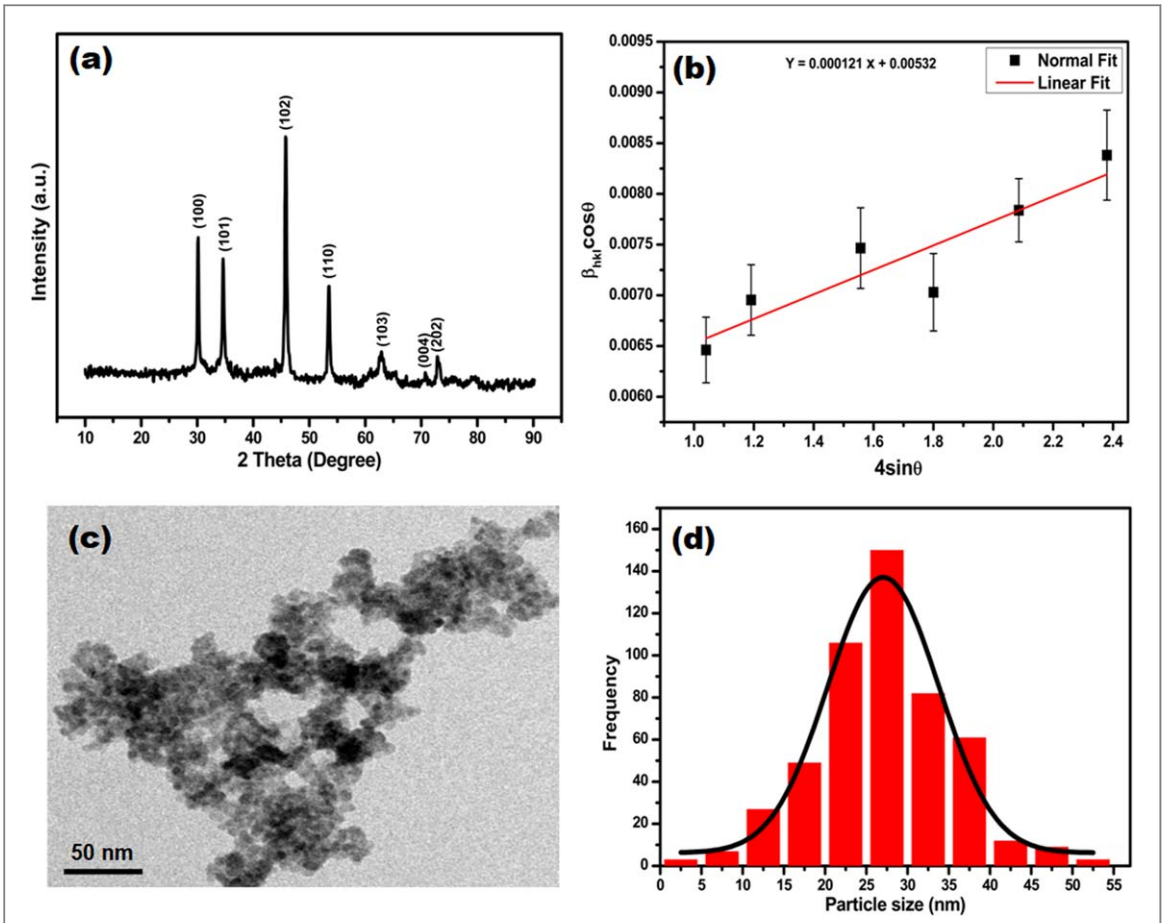

Figure 3. (a) XRD pattern, (b) W-H-UDM plot (c) HRTEM image and (d) histogram showing particle size distribution of NiS NPs.

In general, the instrumental broadening function can be written as,

$$\beta_{total} = \beta_{size} + \beta_{strain} \tag{3}$$

The expression for strain induced peak brodening can be given by,

$$\beta_{strain} = 4\varepsilon \,.\, \tan\theta \tag{4}$$

The total brodening owing to size and strain for a particular peak having *hkl* value can be given as,

$$\beta_{hkl} = \beta_{size} + \beta_{strain} \tag{5}$$

$$\text{Therefore, } \beta_{hkl} = \frac{k\lambda}{D}.\frac{1}{\cos\theta} + 4\varepsilon \,.\, \tan\theta \tag{6}$$

On rearranging equation (6), we have,

$$\beta_{hkl} \,.\, \cos\theta = \frac{k\lambda}{D} + 4\varepsilon.\, \sin\theta \tag{7}$$

Equation (7) is an equation of straight line and is called UDM equation and this is considerable for isotropic nature of crystals [50, 51].

A plot is drawn by taking 4 sin θ values along X-axis and β_{hkl}. cos θ values along Y-axis for most of the intensed peaks as depicted in figure 3(b). In W-H-UDM model, the intercept made by the plot represents the average crystallite size, whereas the slope of the straight line corresponds to the value of the intrinsic strain. From the W-H-UDM method, the average crystallite size and the intrinsic strain are calculated to be around 26 nm and 0.121×10^{-3} respectively. Also, from the figure 3(b), it has been noticed that the slope of the W-H-UDM plot is positive which represents the lattice expansion [51]. Figure 3(c) displays HRTEM image of NiS NPs which shows a quasi-spherical shape with very small aggregations [28]. The particle size histogram based on HRTEM is depicted in figure 3(d). The total numbers of NPs accounted for particle size histogram are 509 per field of view. From this, it can be observed that the average particle size ranges from 20–30 nm which is in good agreement with XRD results. The XRD patterns of pure PVA and PVA/NiS nanocomposite films are represented in figure 4. Figure 4(a) depicts a diffraction peak around $2\theta = 19.67°$ which is ascribed to the semi-crystalline nature of neat PVA ascribing to (101) plane reflections [52–57]. The PVA/NiS nanocomposites (figures 4(b)–(g))

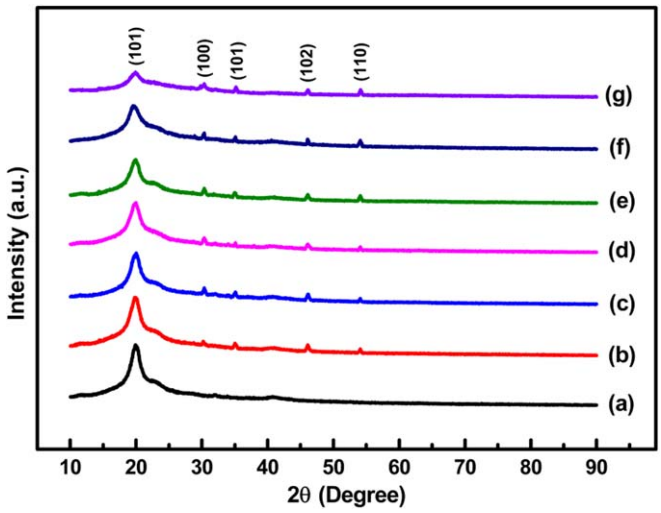

Figure 4. XRD patterns of (a) neat PVA, (b) PVA/NiS nanocomposite films filled with 0.5 wt% NiS NPs, (c) 1.0 wt% NiS NPs, (d) 1.5 wt% NiS NPs, (e) 2.0 wt% NiS NPs, (f) 2.5 wt% NiS NPs and (g) 3.0 wt% NiS NPs.

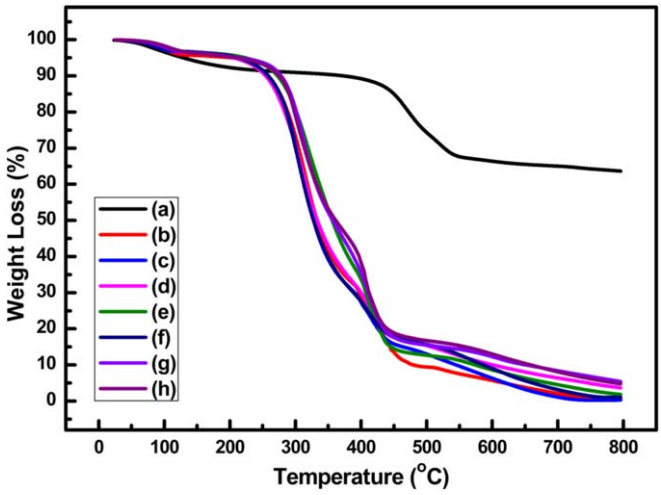

Figure 5. TGA plots of (a) NiS NPs, (b) neat PVA, (c) PVA/NiS nanocomposite films embedded with 0.5 wt% NiS NPs, (d) 1.0 wt% NiS NPs, (e) 1.5 wt% NiS NPs, (f) 2.0 wt% NiS NPs, (g) 2.5 wt% NiS NPs and (h) 3.0 wt% NiS NPs.

also show the broad diffraction peak at $2\theta = 19.82°$ representing the existence of PVA with several additional small peaks at $2\theta = 30.38°$, 35.11°, 45.99° and 54.09° which strongly corroborate the existence of NiS in the nanocomposites. Moreover, it has been noticed that the intensity of the diffraction peak corresponding to PVA is decreased with an increase in the NiS NPs loading in the nanocomposites. This may be due to the possible intermolecular interactions between the nanofiller and the host polymer matrix which tends to decrease within the polymer chains and therefore the degree of crystallinity [58–60].

3.3. Thermal analysis

Figures 5(a)–(h) displays TGA thermograms of NiS NPs, neat PVA and PVA/NiS nanocomposite films. The NiS NPs (figure 5(a)) depict two weight loss stages (overall weight loss is about 36.06%). The first decomposition stage is noticed between the temperatures 39 °C and 350 °C (weight loss about 8.82%) which could be due to the elimination of hydroxide group and residual moisture. The second stage of weight loss about 22.92% occurs in the temperature range 350–540 °C which may be attributed to the gradual decomposition of the sulfur during structural collapse process [61]. The residual mass of NiS NPs is observed to be 63.73%. The neat PVA (figure 5(b)) exhibits three degradation steps (overall weight loss about 99.83%). The first step of degradation (about 4.21% weight loss) is identified in the temperature range 52 °C–130 °C which is because of elimination of hydrolyzed water in the film [62]. The second step of degradation (weight loss about 62.04%) appears between

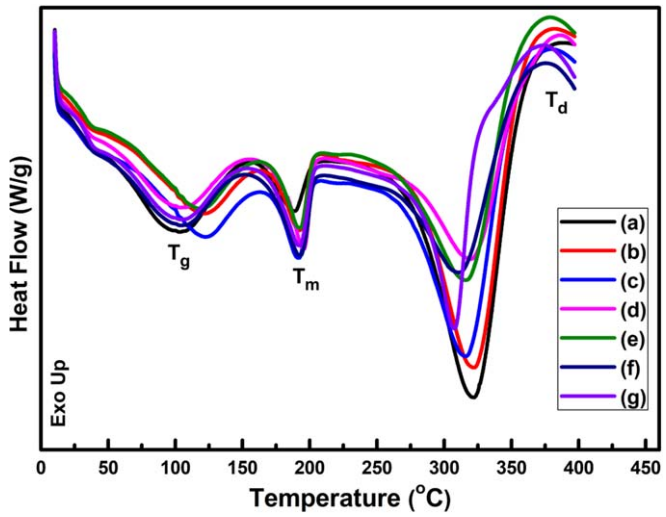

Figure 6. DSC thermographs of (a) neat PVA, (b) PVA/NiS nanocomposite films loaded with 0.5 wt% NiS NPs, (c) 1.0 wt% NiS NPs, (d) 1.5 wt% NiS NPs, (e) 2.0 wt% NiS NPs, (f) 2.5 wt% NiS NPs and (g) 3.0 wt% NiS NPs.

Table 1. T_g, T_m ,$T_{d,}$ ΔH and Cof neat PVA and PVA/NiS nanocomposite films.

Samples	T_g (°C)	T_m (°C)	T_d (°C)	ΔH (J g^{-1})	C (%)
PVA	103.29	187.53	385.09	25.60	18.47
0.5 wt % NiS	121.19	191.66	379.66	30.63	22.10
1 wt % NiS	122.33	192.65	378.79	30.23	21.81
1.5 wt % NiS	104.15	194.69	384.95	36.79	26.54
2 wt % NiS	119.08	191.66	377.92	35.23	25.42
2.5 wt % NiS	105.41	192.52	375.31	41.72	30.10
3 wt % NiS	104.87	192.09	373.58	39.43	28.45

the temperatures 150 °C and 390 °C owing to chain scission, splitting of monomer unit and degradation in the polymer's backbone [63, 64]. The third step of degradation exhibits weight loss about 33.58% above 420 °C which may because of the cleavage of C-C (residual carbon) bond of PVA and complete decomposition of its backbone [63–66]. The PVA/NiS nanocomposite films also show three stages of decomposition (figures 5(c)–(h). The overall weight loss of these nanocomposite films are identified to be about in the range 99.53–93.7%. The first decomposition stage appears between the temperatures 48 °C and 134 °C (weight loss is in the range 3.06%–3.65%) which is ascribed to the removal of adsorbed water present in the nanocomposites. The second stage of decomposition is located in the temperature range 147 °C–403 °C which could be due to the bond scission and splitting of the monomer unit in the backbone of PVA [58]. The weight loss in the second decomposition stage is observed to be in the range 52.99%–67.40%. The third decomposition stage appears above 415 °C (weight loss is in the range 27.68%–37.49%) which is attributed to the further structural decomposition of PVA resulting in the formation of carbonaceous residue consisting of macromolecular fragmentation of both the NiS NPs and PVA [58, 67, 68]. From figures 5(c)–(h), it has been noticed that the final residual mass of the PVA/NiS nanocomposite films isincreased with increase in NiS content (wt %) in the PVA matrix and found to be in the range 1.19%–6.02% whereas for neat PVA, the residual mass is observed to be 0.73% only. This residual mass demonstrates non-degraded polymer chains, alkenes and other organic compounds that existed in the nanocomposites [69]. These results suggest that the PVA/NiS nanocomposite films exhibit better thermal stability as compared with neat PVA. The cause for showing better thermal stability of nanocomposites is the successful inclusion of NiS NPs in the PVA matrix and also good interaction between them. Hence, the incorporation of NiS NPs into PVA restricts the motion of a polymeric chain and consequently decreases the weight loss and results in a sluggish decomposition process [70].

Furthermore, the thermal properties of PVA/NiS nanocomposites were carried out using DSC which gives the information about the effect of nanofiller concentration on glass transition temperature (T_g), melting temperature (T_m), and degradation temperature (T_d) etc on the host polymers [71–73]. Figures 6(a)–(g) displays the DSC thermographs of pure PVA and PVA/NiS nanocomposite films. For all the samples, three endothermic peaks were identified. The first peak ascribed to T_g was identified at 103.29 °C for PVA and in the temperature

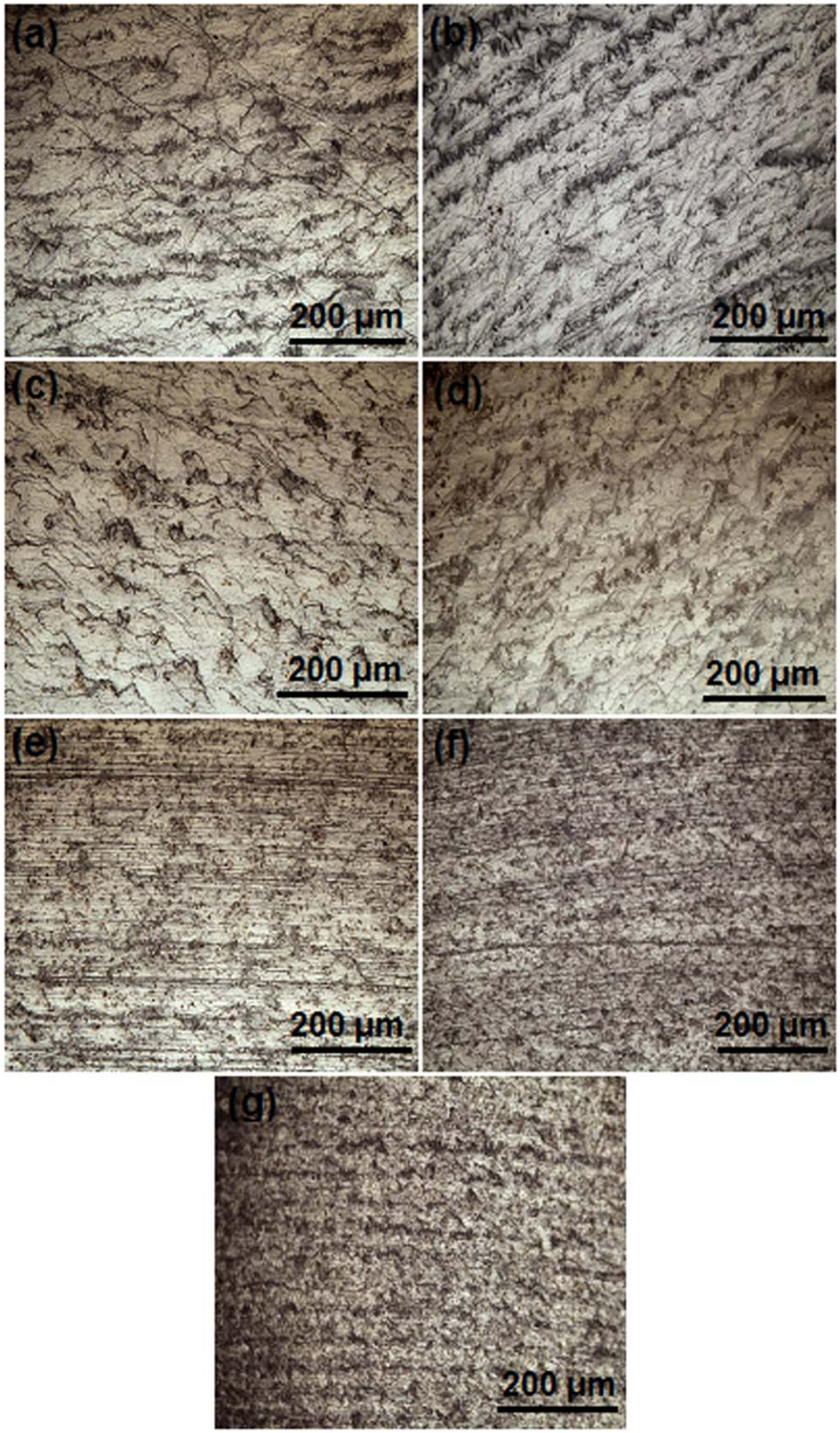

Figure 7. POM images of (a) neat PVA, (b) PVA/NiS nanocomposite films loaded with 0.5 wt% NiS NPs, (c) 1.0 wt% NiS NPs, (d) 1.5 wt% NiS NPs, (e) 2.0 wt% NiS NPs, (f) 2.5 wt% NiS NPs and (g) 3.0 wt% NiS NPs.

range from 104.15 °C–122.33 °C for PVA/NiS nanocomposites. Such peaks may be ascribed to removal of moisture on the surface of the samples [74, 75]. The second peak assigned to T_m is noticed at 187.53 °C for neat PVA [68]. For PVA/NiS nanocomposites, the T_m value lies within the temperature range 191.66 °C–194.69 °C. The slight increase in the T_m values of the nanocomposites was noticed and this is due to confinement effects and

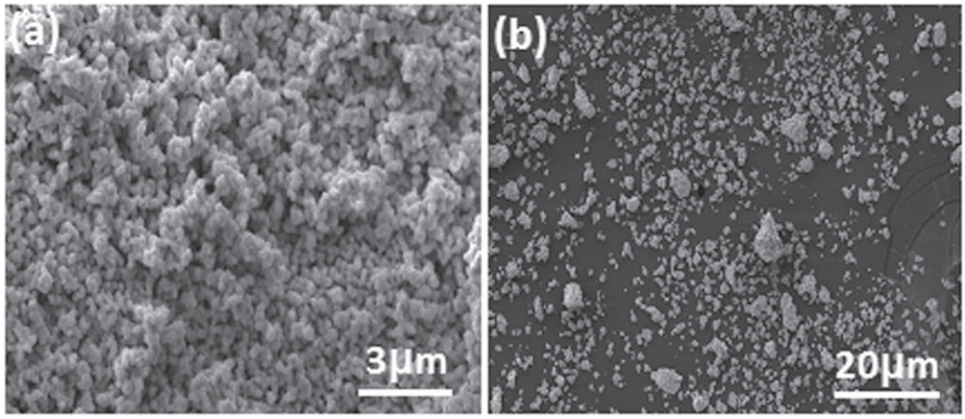

Figure 8. SEM images of NiS NPs at different resolutions.

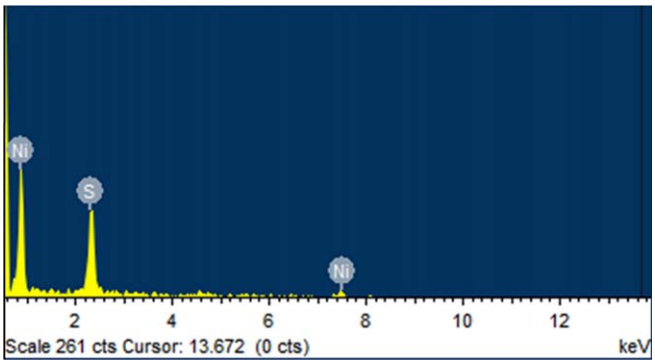

Figure 9. EDAX spectrum of NiS NPs.

interactions between the nanofiller and host polymer matrix [72, 76]. The third endothermic peak appears at the temperature 320.82 °C and in the temperature range 307.58 °C–319.69 °C which is ascribed to pyrolysis of PVA and PVA/NiS nanocomposites respectively. Finally, an additional exothermic peak occurs at 385.09 °C which is attributed to T_d for neat PVA and its value lies in the temperature range 373.58 °C–384.95 °C for PVA/NiS nanocomposites. The degree of crystallinity (C) of the polymer can be calculated from DSC endothermic curves using the following equation by assuming a linear relationship between the endothermal peak area and crystallinity [77].

$$C = \frac{\Delta H}{\Delta H_o} \times 100\% \quad (8)$$

Where C is the crystallinity of a semicrystalline polymer, ΔH is the heat of fusion of a semicrystalline polymer, and ΔH_o is the heat required for melting of 100 % PVA (138.6 J g^{-1}). The endothermic melting transition and the calculated crystallinity of the samples are presented in table 1.

3.4. Morphology and microstructural studies

Figures 7(a)–(g) depicts POM images of neat PVA and PVA/NiS nanocomposite films. The neat PVA film (figure 7(a)) demonstrates a homogeneous and smooth surface morphology. On the other hand, the PVA/NiS nanocomposite films (figures 7(b)–(g) demonstrate rough surface indicating an excellent adhesion between the PVA matrix and the nanofiller [78]. Further, SEM micrographs of NiS NPs, neat PVA and PVA/NiS nanocomposite films were obtained to investigate the microstructure, composition and degree of dispersion of nanofiller in the polymer matrix. Figures 8(a), (b) displays the SEM micrographs of NiS NPs with different magnifications. These images revealed the agglomerated and quasi-spherical shaped NPs. Figure 9 depicts the EDAX spectrum of NiS NPs which confirms the presence of nickel and sulphur in the chemical compositions of NiS. Figures 10(a)–(g) shows SEM images of PVA/NiS nanocomposite films. The neat PVA film depicts smooth and flat surface (figure 10(a)) whereas NPs agglomerations (white spots) were noticed in the SEM micrographs of PVA/NiS nanocomposites at all concentrations with varying degree of dispersion (figures 10(b)–(g)). Moreover, it has been observed that the agglomeration of NiS NPs in the polymer matrix increases with increasing NiS

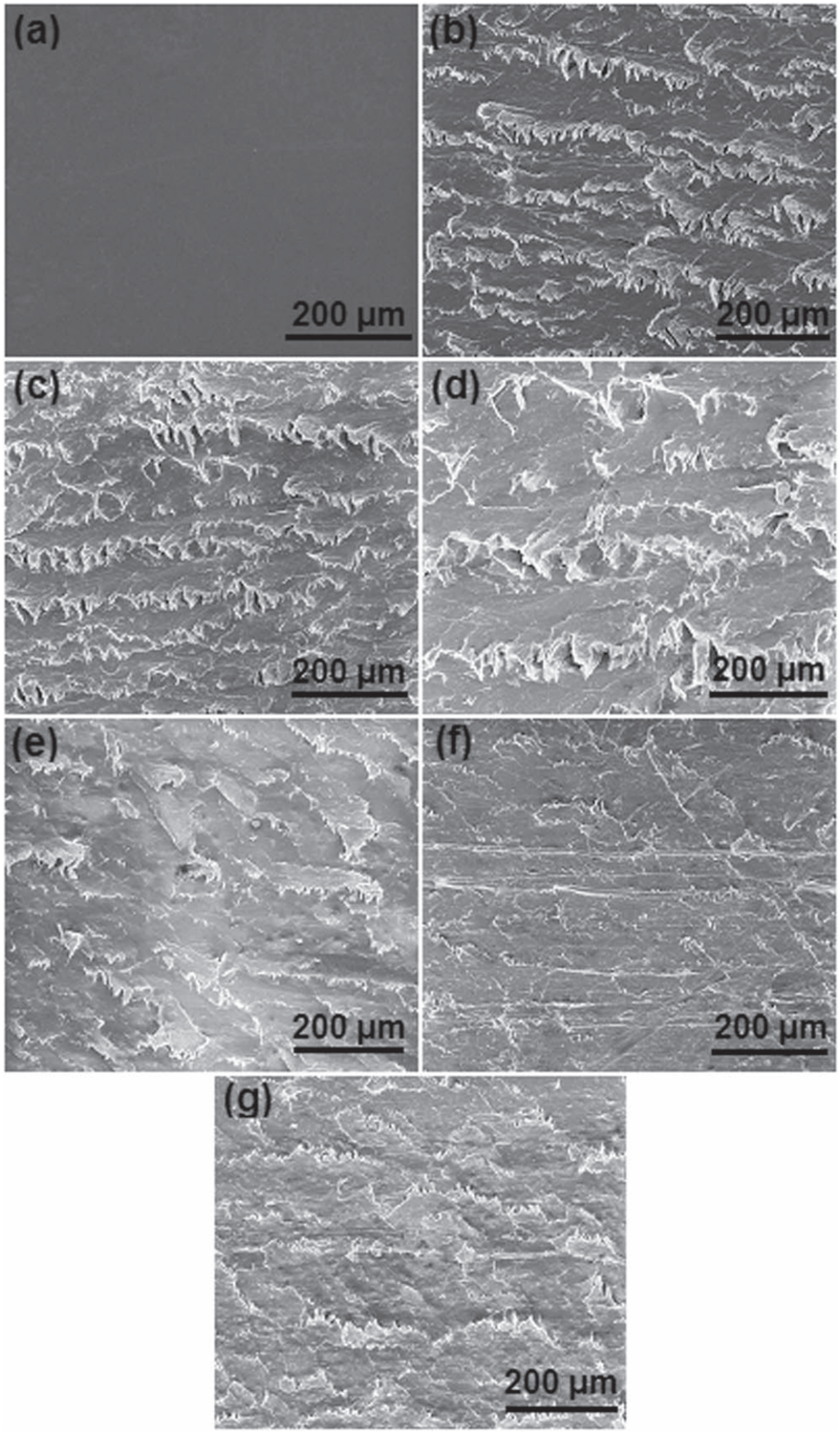

Figure 10. SEM images of (a) neat PVA, (b) PVA/NiS nanocomposite films filled with 0.5 wt% NiS NPs, (c) 1.0 wt% NiS NPs, (d) 1.5 wt% NiS NPs, (e) 2.0 wt% NiS NPs, (f) 2.5 wt% NiS NPs and (g) 3.0 wt% NiS NPs.

content. Finally, the morphology of the PVA/NiS nanocomposite films was investigated using HRTEM and the results are shown in figure 11. The HRTEM images of PVA/NiS nanocomposite films filled with 3 wt% of NiS NPs (figures 11(a)–(d)) revealed that the NiS NPs have been uniformly dispersed in the PVA matrix revealing good compatibility between the polymer matrix and the nanofiller [12].

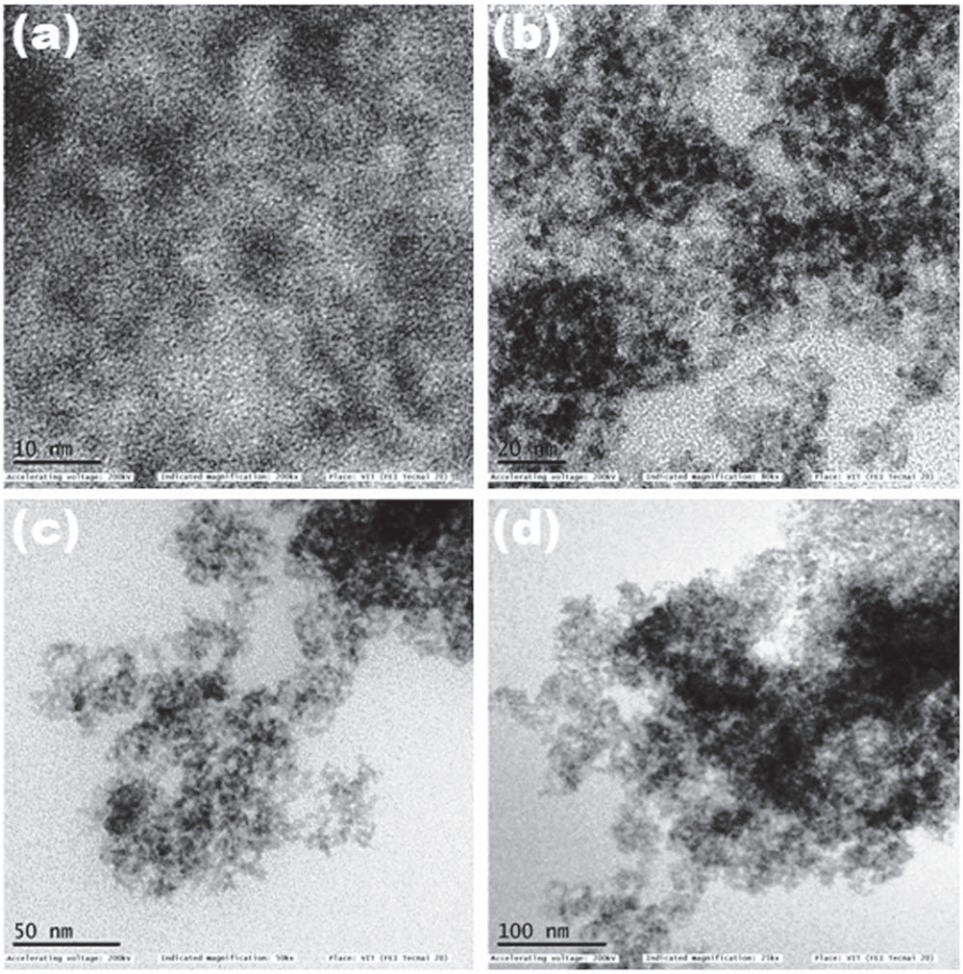

Figure 11. HRTEM images of PVA/NiS nanocomposite film loaded with 3 wt% NiS NPs at different resolutions.

Table 2. ε and tan δ values of PVA/NiS nanocomposite films.

PVA/NiS compositions	ε	tan (δ)
100/0	6.90, 50 Hz, 140 °C	0.22, 50 Hz, 140 °C
99.5/0.5	28.71, 50 Hz, 140 °C	0.38, 50 Hz, 140 °C
99/1.0	60.14, 50 Hz, 140 °C	0.62, 50 Hz, 140 °C
98.5/1.5	68.97, 50 Hz, 140 °C	0.71, 50 Hz, 140 °C
98/2.0	114.79, 50 Hz, 140 °C	0.83, 50 Hz, 140 °C
97.5/2.5	124.22, 50 Hz, 140 °C	0.92, 50 Hz, 140 °C
97/3.0	154.55, 50 Hz, 140 °C	0.98, 50 Hz, 140 °C

3.5. Dielectric studies

The PNCs having higher dielectric constant and lower dielectric loss are essential for energy storage applications [79–81]. As the energy storage capacity of these materials is the key for utilization in energy generating devices, significant interest has been shown in the analysis of dielectric properties of various PNCs [82]. Also, the chain interactions and the polarity of the host polymer may affect the interface between the polymer matrix and the NPs [83]. The dielectric constant (ε) and dielectric loss (tanδ) values of PVA/NiS nanocomposite films are given in table 2. Figures 12(a)–(g) denotes dielectric constant plots of PVA and PVA/NiS nanocomposite films measured at various frequencies (50 Hz-20 MHz) and various temperatures (40 °C–140 °C). From figures 12(a)–(g), it has been observed that both PVA and PVA/NiS nanocomposite films show high dielectric constant values at lower frequencies. The dielectric constant decreases with an increase in frequency which may be attributed to Maxwell-Wagner Sillar (MWS) polarization effect or interfacial polarization effect, which is

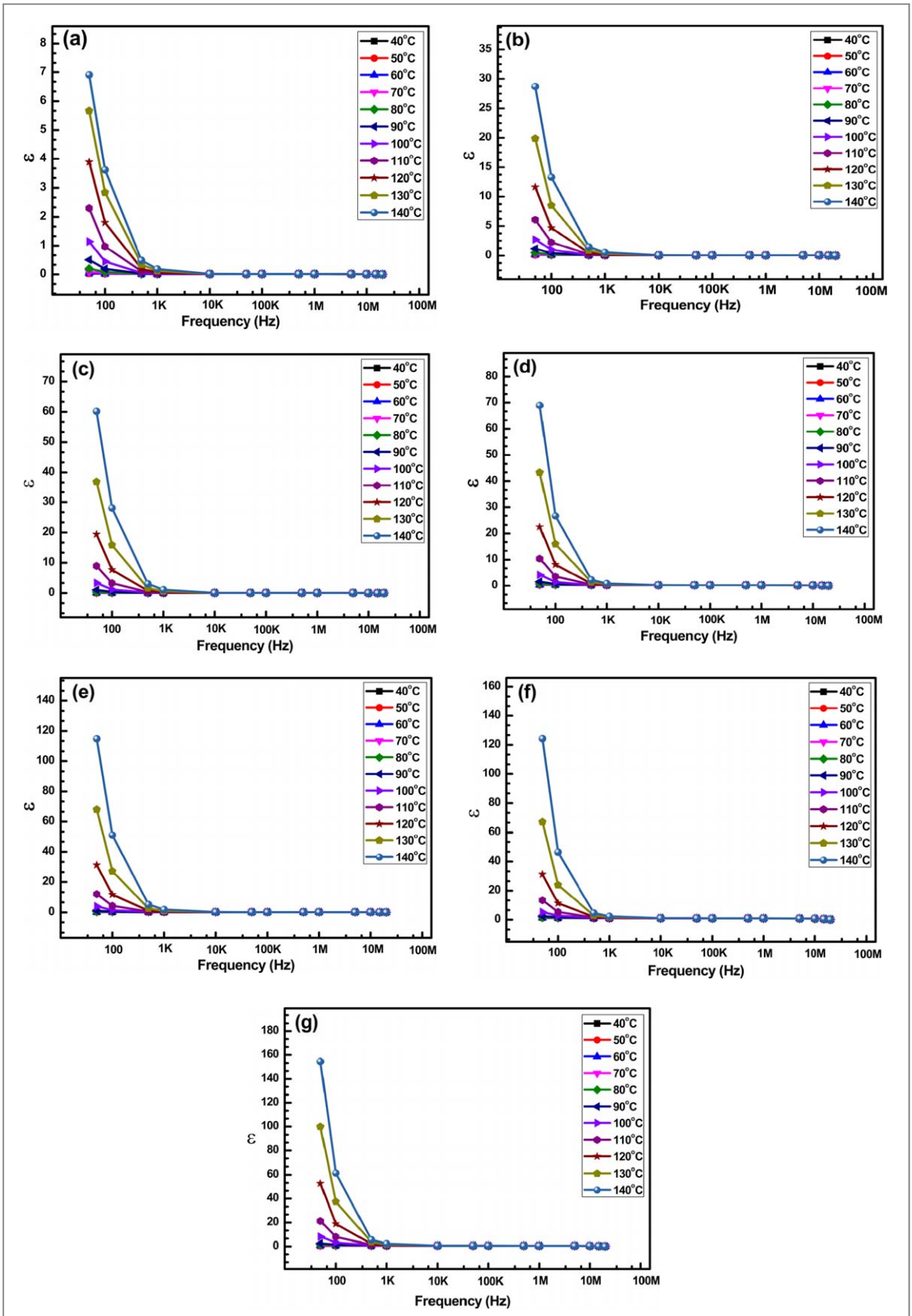

Figure 12. (a): Dielectric constant (ε) plots of neat PVA as a function of frequency at different temperatures. (b): Dielectric constant (ε) plots of PVA/NiS nanocomposite films filled with 0.5 wt% NiS NPs as a function of frequency at different temperatures. (c): Dielectric constant (ε) plots of PVA/NiS nanocomposite films filled with 1.0 wt% NiS NPs as a function of frequency at different temperatures. (d): Dielectric constant (ε) plots of PVA/NiS nanocomposite films filled with 1.5 wt% NiS NPs as a function of frequency at different temperatures. (e): Dielectric constant (ε) plots of PVA/NiS nanocomposite films filled with 2.0 wt% NiS NPs as a function of frequency at different temperatures. (f): Dielectric constant (ε) plots of PVA/NiS nanocomposite films filled with 2.5 wt% NiS NPs as a function of frequency at different temperatures. (g): Dielectric constant (ε) plots of PVA/NiS nanocomposite films filled with 3.0 wt% NiS NPs as a function of frequency at different temperatures.

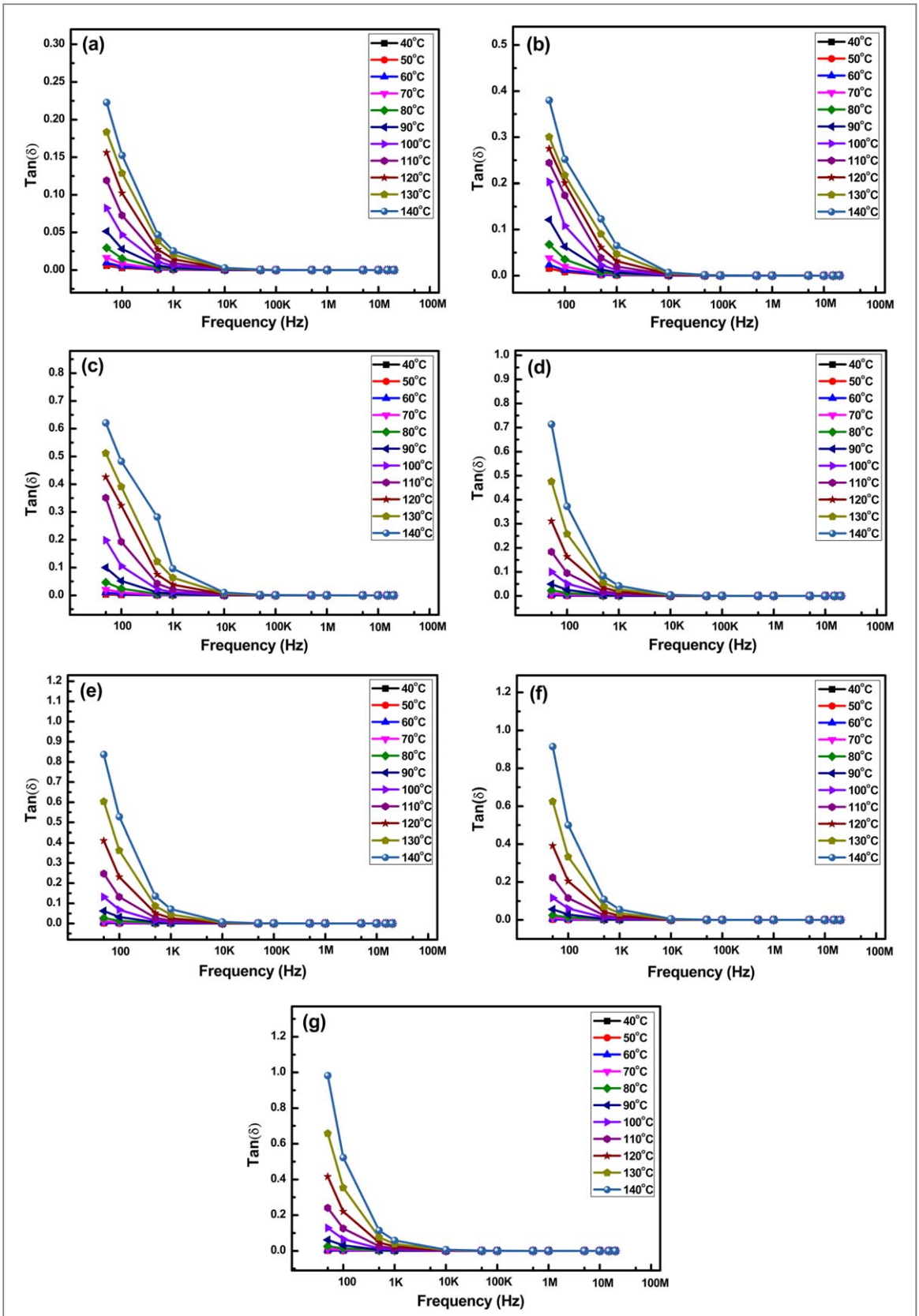

Figure 13. (a): Dielectric loss (Tan(δ)) plots of neat PVA as a function of frequency at different temperatures. (b): Dielectric loss (Tan(δ)) plots of PVA/NiS nanocomposite films with 0.5 wt% NiS NPs loading as a function of frequency at different temperatures. (c): Dielectric loss (Tan(δ)) plots of PVA/NiS nanocomposite films with 1.0 wt% NiS NPs loading as a function of frequency at different temperatures. (d): Dielectric loss (Tan(δ)) plots of PVA/NiS nanocomposite films with 1.5 wt% NiS NPs loading as a function of frequency at different temperatures. (e): Dielectric loss (Tan(δ)) plots of PVA/NiS nanocomposite films with 2.0 wt% NiS NPs loading as a function of frequency at different temperatures. (f): Dielectric loss (Tan(δ)) plots of PVA/NiS nanocomposite films with 2.5 wt% NiS NPs loading as a function of frequency at different temperatures. (g): Dielectric loss (Tan(δ)) plots of PVA/NiS nanocomposite films with 3.0 wt% NiS NPs loading as a function of frequency at different temperatures.

defined as the accumulation of charge carriers at the interface between the polymer matrix and the nanofiller [84, 85]. At higher frequency, the interfacial dipoles do not have enough time to align themselves in the direction of an applied electric field [53, 86, 87]. Also, the MWS effect in polarization is typified by the dependence of frequency and the value of ε in the low-frequency region. At higher frequencies (10 KHz–20 MHz), no significant change in dielectric constant was observed which demonstrating the good frequency stability of samples. Generally, it happens because the dipole orientation is difficult at the higher frequencies [53]. The maximum dielectric constant value was found to be 154.55 (at 50 Hz and at140 °C) for PVA/NiS nanocomposite films reinforced with 3 wt% NiS NPs which is 22 times greater than the dielectric constant value of pure PVA (6.90). This indicates an excellent interfacial adhesion between the nanofiller and the host polymer matrix. Furthermore, it has been noticed that the ε values have increased with an increment in the nanofiller loading in the host polymer matrix. For a dielectric material, tanδ is also one of the significant parameters which give information about the dissipation of energy (loss) of an electromagnetic field. Figures 13(a)–(g) displays the tanδ values of PVA and PVA/NiS nanocomposite films. These nanocomposite films show high values of tanδ at lower frequencies and low tanδ values at higher frequencies which could be due to the interfacial polarization [44, 58]. Moreover, the tanδ values have increased with an increase in NiS loading in the PVA matrix (figures 13(b)–(g)). However, as compared with the ε values, the tanδ values are very low which is very attractive for energy storage device applications [44, 88].

4. Conclusions

In this work, NiS NPs and PVA/NiS nanocomposite films have been successfully prepared via a green synthesis approach and solution casting method respectively. The PVA/NiS nanocomposites were analyzed using various characterization techniques. The FTIR and XRD results revealed that the NiS NPs and PVA have significant interaction with each other. TGA and DSC results evidenced an improvement in the thermal stability of PVA/NiS nanocomposite films as compared with pure PVA film. The POM, SEM and HRTEM results revealed that the morphology and microstructure of PVA/NiS nanocomposites were significantly modified with the addition of NiS NPs in the PVA matrix. Moreover, high ε and low tanδ values obtained for the PVA/NiS nanocomposite films suggesting their potential applications in energy storage devices.

Acknowledgments

The author PL Reddy would like to thank the management of VIT University for providing the facilities for FTIR and XRD analysis through VIT-DST-FIST scheme.

ORCID iDs

Tomáš Kovářík https://orcid.org/0000-0003-4838-4069
Khadheer Pasha S K https://orcid.org/0000-0002-5171-8915

References

[1] Ponnamma D *et al* 2019 Synthesis, optimization and applications of ZnO/Polymer nanocomposites *Mater. Sci. Eng.* C **98** 1210–40
[2] Müller K *et al* 2017 Review on the processing and properties of polymer nanocomposites and nanocoatings and their applications in the packaging, automotive and solar energy fields *Nanomaterials* **7** 74–121
[3] Sankaran S, Deshmukh K, Ahamed M B, Sadasivuni K K, Faisal M and Pasha S K K 2019 Electrical and electromagnetic interference shielding properties of hexagonal boron nitride nanoparticles reinforced polyvinylidene fluoride nanocomposite films *Polym. Plast. Technol. Eng.* **58** 1191–209
[4] Deshmukh K, Ahamed M B, Sadasivuni K K, Ponnamma D, Al-Maadeed M A A, Deshmukh R R, Pasha S K K, Polu A R and Chidambaram K 2016 Fumed SiO_2 nanoparticle reinforced biopolymer blend nanocomposites with high dielectric constant and low dielectric loss for flexible organic electronics *J. Appl. Polym. Sci.* **134** 44427
[5] Sadasivuni K K *et al* 2019 A review on porous polymer nanocomposites for multifunctional electronic applications *Polym. Plast. Technol. Eng.* **58** 1253–94
[6] Pandey M, Joshi G M, Deshmukh K, Khutia M and Ghosh N N 2014 Optimized AC conductivity correlated to structure, morphology and thermal properties of PVDF/PVA/Nafion composites *Ionics* **20** 1427–33
[7] Mohanapriya M K, Deshmukh K, Kadlec J, Sadasivuni K K, Faisal M, Nambiraj N A and Pasha S K K 2020 Dynamic mechanical analysis and broadband electromagnetic interference shielding characteristics of poly (vinyl alcohol)-poly (4-styrenesulfonic acid)-titanium dioxide nanoparticles based tertiary nanocomposites *Polym. Plast. Technol. Eng.* **59** 847–63
[8] Deshmukh K, Ahamed M B, Deshmukh R R, Pasha S K K, Chidambaram K, Sadasivuni K K, Ponnamma D and Al-Maadeed M A A 2016 Eco-friendly synthesis of graphene oxide reinforced hydroxypropyl methylcellulose (HPMC)/polyvinyl alcohol (PVA) blend nanocomposites filled with zinc oxide (ZnO) nanoparticles for high-k capacitor applications *Polym. Plast. Tech. Eng.* **55** 1240–53

[9] Ahmad J, Deshmukh K, Habib M and Hagg M B 2014 Influence of TiO_2 nanoparticles on the morphological, thermal and solution properties of PVA/TiO_2 nanocomposite membranes *Arab. J. Sci. Eng.* **39** 6805–14

[10] Joshi G M and Deshmukh K 2016 Study of conjugated polymer/graphene oxide nanocomposites as flexible dielectric medium *J. Mater. Sci.: Mater. Electron.* **27** 3397–409

[11] Joseph J, Deshmukh K, Chidambaram K, Faisal M, Selvarajan E, Sadasivuni K K, Ahamed M B and Pasha S K K 2018 Dielectric and electromagnetic interference shielding properties of germanium dioxide nanoparticle reinforced poly (vinylchloride) and poly (methylmethacrylate) blend nanocomposites *J. Mater. Sci.: Mater. Electron.* **29** 20172–88

[12] Reddy P L, Deshmukh K, Chidambaram K, Nazeer A M M, Sadasivuni K K, Kumar Y R, Lakshmipathy R and Pasha S K K 2019 Dielectric properties of polyvinyl alcohol (PVA) nanocomposites filled with green synthesized zinc sulphide (ZnS) nanoparticles *J. Mater. Sci.: Mater. Electron.* **30** 4676–87

[13] Deshmukh K and Joshi G M 2015 Embedded capacitor applications of graphene oxide reinforced poly(3,4-ethylenedioxythiophene)-tetramethacrylate (PEDOT-TMA) composites *J. Mater. Sci.: Mater. Electron.* **26** 5896–909

[14] Barber P, Balasubramanian S, Anguchamy Y, Gong S, Wibowo A, Gao H, Ploehn H J and Loye H C Z 2009 Polymer composite and nanocomposite dielectric materials for pulse power energy storage *Materials* **2** 1697–733

[15] Zhang Y, Wang Y, Deng Y, Li M and Bai J 2012 Enhanced dielectric properties of ferroelectric polymer composites induced by metal-semiconductor Zn-ZnO core–shell structure *ACS Appl. Mater. Interfaces* **4** 65–8

[16] Bhadra D, Masud M G, Sarkar S, Sannigrahi J, De S K and Chaudhur B K 2012 Synthesis of PVDF/$BiFeO_3$ nanocomposite and observation of enhanced electrical conductivity and low-loss dielectric permittivity at percolation threshold *J. Polym. Sci. Polym. Phys.* **50** 572–9

[17] Deshmukh K, Ahamed M B, Deshmukh R R, Sadasivuni K K, Ponnamma D, Pasha S K K, Al-Maadeed M A A, Polu A R and Chidambaram K 2017 Eeonomer 200F®: A high-performance nanofiller for polymer reinforcement-Investigation of the structure, morphology and dielectric properties of polyvinyl alcohol/Eeonomer 200F® nanocomposites for embedded capacitor applications *J. Electron. Mater.* **46** 2406–18

[18] Sankaran S, Deshmukh K, Ahamed M B and Pasha S K K 2018 Recent Advances in electromagnetic interference shielding properties of metal and carbon filler reinforced flexible polymer composites: a review *Composites Part A: Appl. Sci. Manuf.* **114** 49–71

[19] Mahendia S, Tomar A K and Kumar S 2010 Electrical conductivity and dielectric spectroscopic studies of PVA-Ag nanocomposite films *J. Alloy. Compd.* **508** 406–11

[20] Rashmi S H, Raizada A, Madhu G M, Kittur A A, Suresh R and Sudhina H K 2015 Influence of zinc oxide nanoparticles on structural and electrical properties of polyvinyl alcohol films *Plast. Rubber Compos.* **44** 33–9

[21] Ambrosio R, Carrillo A, Mota M D L L, Torre K D L, Torrealba R, Moreno M, Vazquez H, Flores J and Vivaldo I 2018 Polymeric nanocomposites membranes with high permittivity based on PVA-ZnO nanoparticles for potential applications in flexible electronics *Polymers (Basel)* **10** 1370

[22] Lai C H, Lu M Y and Chen L J 2012 Metal sulfide nanostructures: synthesis, properties and applications in energy conversion and storage *J. Mater. Chem.* **22** 19–30

[23] Chi W S, Han J W, Yang S, Roh D K, Lee H and Kim J H 2012 Employing electrostatic self-assembly of tailored nickel sulfide nanoparticles for quasi-solid-state dye-sensitized solar cells with Pt-free counter electrodes *Chem. Commun.* **48** 9501–3

[24] Zhu T, Wu H B, Wang Y, Xu R and Lou X W D 2012 Formation of 1D hierarchical structures composed of Ni_3S_2 nanosheets on CNTs backbone for supercapacitors and photocatalytic H_2 production *Adv. Energy Mater.* **2** 1497–502

[25] Shajudheen M V P, Kumar S V, Rani A K, Maheswari U A and Kumar S S 2016 Structural and optical properties of NiS nanoparticles synthesized by chemical precipitation method *Int. J. Innov. Res. Sci. Eng. Technol.* **5** 15099–103

[26] Salavati-Niasari M, Davar F and Mazaheri M 2009 Synthesis, characterization and magnetic properties of NiS_{1+x} nanocrystals from [bis (salicylidene)nickel(II)] as new precursor *Mater. Res. Bull.* **44** 2246–51

[27] Zhang J, Xu C, Zhang D, Zhao J, Zheng S, Su H, Wei F, Yuan B and Fernandez C 2017 Facile synthesis of a nickel sulfide (NiS) hierarchical flower for the electrochemical oxidation of H_2O_2 and the methanol oxidation reaction (MOR) *J. Electrochem. Soc.* **164** B92–6

[28] Karthikeyan R, Thangaraju D, Prakash N and Hayakawa Y 2015 Single-step synthesis and catalytic activity of structure-controlled Nickel sulfide nanoparticles *Cryst. Eng. Comm.* **17** 5431–9

[29] Singh J, Dutta T, Kim K, Rawat M, Samddar P and Kumar P 2018 Green synthesis of metals and their oxide nanoparticles: applications for environmental remediation *J. Nanobiotechnol.* **16** 84

[30] Yan D, Zhang H, Chen L, Zhu G, Wang Z, Xu H and Yu A 2014 Supercapacitive properties of Mn_3O_4 nanoparticles bio-synthesized from banana peel extract *RSC Adv.* **4** 23649–52

[31] Yuliarto B, Septiani N L W, Kaneti Y V K, Iqbal M, Gumilar G, Kim M, Na J, Wu K C W and Yamauchi Y 2019 Green synthesis of metal oxide nanostructures using naturally occurring compounds for energy, environmental, and bio-related applications *New J. Chem.* **43** 15846–56

[32] Vaseghi Z, Nematollahzadeh A and Tavakoli O 2018 Green methods for the synthesis of metal nanoparticles using biogenic reducing agents: a review *Rev. Chem. Eng.* **34** 529–59

[33] Ibrahim H M M 2015 Green synthesis and characterization of silver nanoparticles using banana peel extract and their antimicrobial activity against representative microorganisms *J. Radiat. Res. Appl. Sci.* **8** 265–75

[34] Kanude K R and Jain P 2017 Biosynthesis of CdS nanoparticles using Murraya Koenigii leaf extract and their biological studies *Int. J. Sci. Res. Multidiscip. Studies* **3** 5–10

[35] Hudlikar M, Joglekar S, Dhaygude M and Kodam K 2012 Latex-mediated synthesis of ZnS nanoparticles: green synthesis approach *J. Nanopart. Res.* **18** 865

[36] Sidhu J S and Zafar T A 2018 Bioactive compounds in banana fruits and their health benefits *Food Qual. Saf.* **2** 183–8

[37] Emaga T H, Andrianaivo R H, Wathelet B, Tchango J T and Paquot M 2007 Effects of the stage of maturation and varieties on the chemical composition of banana and plantain peels *Food Chem.* **103** 590–600

[38] Bankar A, Joshi B, Kumar A R and Zinjarde S 2010 Banana peel extract mediated novel route for the synthesis of silver nanoparticles *Colloid. Surf. A Physicochem. Eng. Asp.* **368** 58–63

[39] Ponnamma D, Parangusan H, Deshmukh K, Kar P, Muzaffar A, Pasha S K K, Ahamed M B and Al-Maadeed M A A 2020 Green synthesized materials for sensor, actuator, energy storage and energy generation: a review *Polym. Plast. Technol. Eng.* **59** 1–62

[40] Molla A, Sahu M and Hussain S 2016 Synthesis of tunable band gap semiconductor nickel sulphide nanoparticles: rapid and round the clock degradation of organic dyes *Sci. Rep.* **6** 26034

[41] Sobhani A and Salavati-Niasari M 2013 Synthesis, characterization, optical and magnetic properties of a nickel sulfide series by three different methods *Superlattice Microst.* **59** 1–12

[42] Fazli Y, Pourmortazavi S M, Kohsari I and Sadeghpur M 2014 Electrochemical synthesis and structure characterization of nickel sulfide nanoparticles *Mater. Sci. Semicond. Process.* **27** 362–7
[43] Choo K, Ching Y C, Chuah C H, Julai S and Liou N 2016 Preparation and Characterization of Polyvinyl alcohol-Chitosan composite films reinforced with cellulose nanofiber *Materials* **9** 644
[44] Deshmukh K, Ahamed M B, Deshmukh R R, Pasha S K K, Sadasivuni K K, Ponnamma D and Chidambaram K 2016 Synergistic effect of vanadium pentoxide and graphene oxide in polyvinyl alcohol for energy storage application *Eur. Polym. J.* **76** 14–27
[45] Kumar K N, Padma R, Rao J L and Kang M 2016 Dazzling green emission from graphene oxide nanosheet-embedded co-doped Ce^{3+} and Tb^{3+}: PVA polymer nanocomposites for photonic applications *RSC Adv.* **6** 54525–38
[46] Deshmukh K, Ahamed M B, Pasha S K K, Deshmukh R R and Bhagat P R 2015 Highly dispersible graphene oxide reinforced polypyrrole/polyvinyl alcohol blend nanocomposites with high dielectric constant and low dielectric loss *RSC Adv.* **5** 61933–45
[47] Kharazmi A, Faraji N, Hussin R M, Saion E, Yunus W M M and Behzad K 2015 Structural, optical, opto-thermal and thermal properties of ZnS–PVA nanofluids synthesized through a radiolytic approach *Beilstein J. Nanotechnol.* **6** 529–36
[48] Fazli Y, Pourmortazavi S M, Kohsari I, Karimi M S and Tajdari M 2016 Synthesis, characterization and photocatalytic property of nickel sulfide nanoparticles *J. Mater. Sci.: Mater. Electron.* **27** 7192–9
[49] Saeed S and Rashid N 2015 Growth and characterization of semiconducting nickel sulfide nanocrystals from air-stable single source metal organic precursors *Cogent. Chem.* **1** 1030195
[50] Venkateswarlu K, Bose A C and Rameshbabu N 2010 X-ray peak broadening studies of nanocrystalline hydroxyapatite by Williamson–Hall analysis *Physica.* B **405** 4256–61
[51] Nath D, Singh F and Das R 2020 X-ray diffraction analysis by Williamson-Hall, Halder-Wagner and size-strain plot methods of CdSe nanoparticles- a comparative study *Mater. Chem. Phys.* **239** 122021
[52] Deshmukh K, Ahmad J and Hagg M B 2014 Fabrication and characterization of polymer blends consisting of cationic polyallylamine and anionic polyvinyl alcohol *Ionics* **20** 957–67
[53] Koteswararao J, Abhishek R, Satyanarayana S V, Madhu G M and Venkatesham V 2016 Influence of cadmium sulfide nanoparticles on structural and electrical properties of polyvinyl alcohol films *Express Polym. Lett.* **10** 883–94
[54] Friedlander H N, Harris H E and Pritchard J G 2003 Structure-property relationships of poly(vinyl alcohol). I. Influence of polymerization solvents and temperature on the structure and properties of poly (vinyl alcohol) derived from poly(vinyl acetate) *J. Polym. Sci., Part A: Polym. Chem.* **4** 649–64
[55] Mohanapriya M K, Deshmukh K, Ahamed M B, Chidambaram K and Pasha S K K 2016 Zeolite 4A filled poly (3, 4-ethylenedioxythiophene): (polystyrenesulfonate) (PEDOT: PSS) and polyvinyl alcohol (PVA) blend nanocomposites as high-k dielectric materials for embedded capacitor applications *Adv. Mater. Lett.* **7** 996–1002
[56] Qian X F, Yin J, Guo X X, Yang Y F, Zhu Z K and Lu J F 2000 Polymer-inorganic nanocomposites prepared by hydrothermal method: PVA/ZnS, PVA/CdS, preparation and characterization *J. Mater. Sci. Lett.* **19** 2235–7
[57] Pawde S M, Deshmukh K and Parab S 2008 Preparation and characterization of Poly(vinyl alcohol) and gelatin blend films *J. Appl. Polym. Sci.* **109** 1328–37
[58] Deshmukh K, Ahamed M B, Deshmukh R R, Bhagat P R, Pasha S K K, Bhagat A, Shirbhate R, Telare F and Lakhani C 2016 Influence of K_2CrO_4 doping on the structural, optical and dielectric properties of Polyvinyl alcohol/K_2CrO_4 composite films *Polym. Plast. Technol. Eng.* **55** 231–41
[59] Qian X F, Yin J, Huang J C, Yang X X, Guo Y F and Zhu Z K 2001 The preparation and characterization of PVA/Ag_2S nanocomposite *Mater. Chem. Phys.* **68** 95–7
[60] Onwudiwe D C, Krüger T P J, Oluwatobi O S and Strydom C A 2014 Nanosecond laser irradiation synthesis of CdS nanoparticles in a PVA system *Appl. Surf. Sci.* **290** 18–26
[61] Guo H, Ke Y, Wang D, Lin K, Shen R, Chen J and Weng W 2013 Efficient adsorption and photocatalytic degradation of congo red onto hydrothermally synthesized NiS nanoparticles *J. Nanopart. Res.* **15** 1475
[62] Thangamani G J, Deshmukh K, Chidambaram K, Ahamed M B, Sadasivuni K K, Ponnamma D, Faisal M, Nambiraj N A and Pasha S K K 2018 Influence of CuO nanoparticles and graphene nanoplatelets on the sensing behaviour of poly(vinyl alcohol) nanocomposites for the detection of ethanol and propanol vapors *J. Mater. Sci.: Mater. Electron.* **29** 5186–205
[63] Deshmukh K, Ahamed M B, Sadasivuni K K, Ponnamma D, Al-Maadeed M A A, Pasha K K K, Deshmukh R R and Chidambaram K 2017 Graphene oxide reinforced poly (4-styrenesulfonic acid)/polyvinyl alcohol blend composites with enhanced dielectric properties for portable and flexible electronics *Mater. Chem. Phys.* **186** 188–201
[64] Thangamani G J *et al* 2017 White graphene reinforced polypyrrole and poly(vinyl alcohol) blend nanocomposites as chemoresistive sensors for roomtemperature detection of liquid petroleum gases *Microchim. Acta* **184** 3977–87
[65] Wang J, Gao C, Zhang Y and Wan Y 2010 Preparation and *in vitro* characterization of BC/PVA hydrogel composite for its potential use as artificial cornea biomaterial *Mater. Sci. Eng.* C **30** 214–8
[66] Osuntokun J and Ajibade P A 2016 Structural and thermal studies of ZnS and CdS nanoparticles in polymer matrices *J. Nanomater.* **2016** 1–14
[67] Singh R, Kulkarni S G and Naik N H 2013 Effect of nano sized transition metal salts and metals on thermal decomposition behavior of polyvinyl alcohol *Adv. Mater. Lett.* **4** 82–8
[68] Khan M M R, Pal S, Hoque M M, Alam M R, Younus M and Hisatoshi K 2019 Simple fabrication of PVA-ZnS composite films with superior photocatalytic performance: Enhanced luminescence property, morphology, and thermal stability *ACS Omega* **4** 6144–53
[69] Gilman J W, VanderHart D L and Kashiwagi T 1995 Thermal decomposition chemistry of poly(vinyl alcohol) *ACS Symp. Ser.* **599** 161–85
[70] Leszczynska A, Njuguna J A K, Pielichowski K and Banerjee J R 2007 Polymer/montmorillonite nanocomposites with improved thermal properties: Part I. Factors influencing thermal stability and mechanisms of thermal stability improvement *Thermochim. Acta* **453** 75–96
[71] Guo Z *et al* 2010 Effects of iron oxide nanoparticles on polyvinyl alcohol: interfacial layer and bulk nanocomposites thin film *J. Nanopart. Res.* **12** 2415–26
[72] Singhal A, Kaur M, Dubey K A, Bhardwaj Y K, Jain D, Pillai C G S and Tyagi A K 2012 Polyvinyl alcohol-In_2O_3 nanocomposite films: synthesis, characterization and gas sensing properties *RSC Adv.* **2** 7180–9
[73] Kuljanin J, Čomor M I, Djoković V and Nedeljković J M 2006 Synthesis and characterization of nanocomposite of polyvinyl alcohol and lead sulfide nanoparticles *Mater. Chem. Phys.* **95** 67–71
[74] Alhazime A A, Mohamed M B and Abdel-Kader M H 2019 Effect of $Zn_{1-x}Mg_xS$ doping on structural, thermal and optical properties of PVA *J. Inorg. Organomet. Polym.* **29** 436–43

[75] Radoičić M B, Šaponjić Z V, Marinović-Cincović M T, Ahrenkiel S P, Bibić N M and Nedeljković J M 2012 The influence of shaped TiO_2 nanofillers on the thermal properties of poly(vinyl alcohol) *J. Serb. Chem. Soc.* **77** 699–714
[76] Peng Z, Kong L X and Li S D 2005 Thermal properties and morphology of a poly(vinyl alcohol)/silica nanocomposite prepared with a self-assembled monolayer technique *J. Appl. Polym. Sci.* **96** 1436–42
[77] Tutgun M S, Sinirlioglu D, Celik S U and Bozkurt A 2015 Investigation of nanocomposite membranes based on crosslinked poly(vinyl alcohol)-sulfosuccinic acid ester and hexagonal boron nitride *J. Polym. Res.* **22** 47–57
[78] Pasha S K K, Deshmukh K, Ahamed M B, Chidambaram K, Mohanapriya M K and Nambiraj N A 2015 Investigation of microstructure, morphology, mechanical, and dielectric properties of PVA/PbO nanocomposites *Adv. Polym. Techonol.* **36** 352–61
[79] Karan S K, Das A K, Bera R, Paria S, Maitra A, Shrivastava N K and Khatua B B 2016 Effect of γ-PVDF on enhanced thermal conductivity and dielectric property of Fe-rGO incorporated PVDF based flexible nanocomposite film for efficient thermal management and energy storage applications *RSC Adv.* **6** 37773–83
[80] Ponnamma D, Erturk A, Parangusan H, Deshmukh K, Ahamed M B and Al-Maadeed M A A 2018 Stretchable quaternary phasic PVDF-HFP nanocomposite films containing graphene-titania-$SrTiO_3$ for mechanical energy harvesting *Emergent Mater.* **1** 55–65
[81] Mohanapriya M K, Deshmukh K, Chidambaram K, Ahamed M B, Sadasivuni K K, Ponnamma D, Al-Maadeed M A A, Deshmukh R R and Pasha S K K 2017 Polyvinyl Alcohol (PVA)/polystyrene sulfonic acid (PSSA)/carbon black nanocomposite for flexible energy storage device applications *J. Mater. Sci.: Mater. Electron.* **28** 6099–111
[82] Al-Saygh A, Ponnamma D, Al-Maadeed M A A, Vijayan P P, Karim A and Hassan M K 2017 Flexible pressure sensor based on PVDF nanocomposites containing reduced graphene oxide-titania hybrid nanolayers *Polymers* **9** 33
[83] Deshmukh K, Ahamed M B, Sadasivuni K K, Ponnamma D, Deshmukh R R, Trimukhe A M, Pasha S K K, Polu A R, Al-Maadeed M A A and Chidambaram K 2017 Solution-processed white graphene-reinforced ferroelectric polymer nanocomposites with improved thermal conductivity and dielectric properties for electronic encapsulation *J. Polym. Res.* **24** 27
[84] Xia X, Zhong Z and Weng G J 2017 Maxwell–Wagner–Sillars mechanism in the frequency dependence of electrical conductivity and dielectric permittivity of graphene-polymer nanocomposites *Mech. Mater.* **109** 42–50
[85] Deshmukh K, Ahamed M B, Deshmukh R R, Pasha S K K, Sadasivuni K K, Ponnamma D and Al-Maadeed M A A 2017 Striking multiple synergies in novel three-phase fluoropolymer nanocomposites by combining titanium dioxide and graphene oxide as hybrid fillers *J. Mater. Sci.: Mater. Electron.* **28** 559–75
[86] Dutta P, Biswas S and De S K 2002 Dielectric relaxation in polyaniline-polyvinyl alcohol composites *Mater. Res. Bull.* **37** 193–200
[87] Lu J, Moon S K, Kim B K and Wang C P 2007 High dielectric constant polyaniline/epoxy composites via *in situ* polymerization for embedded capacitor applications *Polymer* **48** 1510–6
[88] Luo H, Zhou X, Ellingford C, Zhang Y, Chen S, Zhou K, Zhang D, Bowen C R and Wan C 2019 Interface design for high energy density polymer nanocomposites *Chem. Soc. Rev.* **48** 4424–65